Supplement of Earth Syst. Sci. Data, 18, 1813–1832, 2026
https://doi.org/10.5194/essd-18-1813-2026-supplement

Open Access Earth System Science Data

Supplement of

All-day global cloud physical properties products with 0.07° resolution retrieved from geostationary satellite imagers covering the period from 2000 to 2022

Lingxiao Zhao et al.

Correspondence to: Feng Zhang (fengzhang@fudan.edu.cn)

Supplement

Contents of this file

Table S1 to Section 3.2

Text S1 to Section 2.2

Figure S1-S4 to Section 3.5

Introduction

This supplementary material: Table S 1 presents the results of the ablation experiments for Cloud-SmaAtUNet and Cloud-RF Text S 1 details the image sliding window fusion strategy. Fig. S 1, Fig. S 2, Fig. S 3, and Fig. S 4 in the article comprise the complete DaYu-GCP DJF, MAM, JJA, and SON seasonal average results for 2020–2022.

Table S1

Table S 1. Cloud-SmaAtUNet and Cloud-RF cloud classification retrieval accuracy under different input groups.

Group	Cloud-SmaAtUNet (%)			Cloud-RF (%)		
	Clear sky	Water cloud	Ice cloud	Clear sky	Water cloud	Ice cloud
1	81.52	80.21	86.38	78.93	73.44	85.19
2	78.86	79.43	83.96	73.52	72.05	82.77
3	66.06	63.64	68.16	61.56	59.42	63.72

Text S1

Image sliding window fusion strategy

The Cloud-SmaAtUNet model was trained using a large number of image samples with a matrix size of 64×64 pixels. Therefore, when reconstructing the local prediction results of 64×64 pixels into a complete global cloud physical properties product image based on implicit prior knowledge (training weights), a certain stitching strategy needs to be adopted. To avoid gaps between adjacent prediction blocks, a sliding window fusion strategy based on linear weights is used.

First, the full image size: $H \times W$. PATCH: $P = 64$. STRIDE: $S = 10$. Since the image size may not be a multiple of PATCH, it is necessary to use rounding up to fill in $H_2 \times W_2$:

$$H_2 = \left\lceil \frac{H}{P} \right\rceil P, W_2 = \left\lceil \frac{W}{P} \right\rceil P \quad (1)$$

The starting coordinates and relative coordinates of the window are (i, j) and (x', y'), respectively.

$$(i, j),\ 0 \le i \le H_2 - P, ; 0 \le j \le W_2 - P \quad (2)$$

$$(x', y'),\ 0 \le x', y' \le P - 1 \quad (3)$$

The weight matrix is composed of piecewise linear functions in the row and column directions. When adjacent blocks exist at the window boundaries, the weights in the boundary regions transition linearly from 0 to 1 (left/top boundary) or from 1 to 0 (right/bottom boundary). By summing the weighted prediction values of the overlapping regions and normalizing them, a seamless stitched image is ultimately formed. The vertical weights $w_y^{(i)}(x')$ and horizontal weights $w_x^{(j)}(y')$ are respectively:

$$w_y^{(i)}(x') = \begin{cases} 0, & i = 0, \\ \frac{x'}{S-1}, & i > 0, 0 \le x' < S, \\ 1, & S \le x' < P - S, \\ \frac{P-1-x'}{S-1}, & i + P < H_2, P - S \le x' < P, \\ 0, & \text{Otherwise.} \end{cases} \quad (4)$$

$$w_x^{(j)}(y') = \begin{cases} 0, & j = 0, \\ \frac{y'}{S-1}, & j > 0, 0 \le y' < S, \\ 1, & S \le y' < P - S, \\ \frac{P-1-y'}{S-1}, & j + P < W_2, P - S \le y' < P, \\ 0, & \text{Otherwise.} \end{cases} \quad (5)$$

The final weight matrix W is constructed by the outer product of vertical weights and horizontal weights:

$$\mathrm{W}_{i,j}(x', y') = w_y^{(i)}(x') \cdot w_x^{(j)}(y') \quad (6)$$

Where i and j are the starting position indices of the window in the filled large image, $x' = x - i,\ y' = y - j, x', y' \in [0, P-1]$. The contributions of each window, $P_{i,j}$ (i.e., the predicted value at the relative coordinates (x', y') within window (i, j)), are weighted and normalized to obtain the final image:

$$I(x,y) = \frac{\sum_{i,j} \mathrm{W}_{i,j}(x-i,y-j) \cdot P_{i,j}(x-i,y-j)}{\sum_{i,j} \mathrm{W}_{i,j}(x-i,y-j)} \quad (7)$$

Figure S1

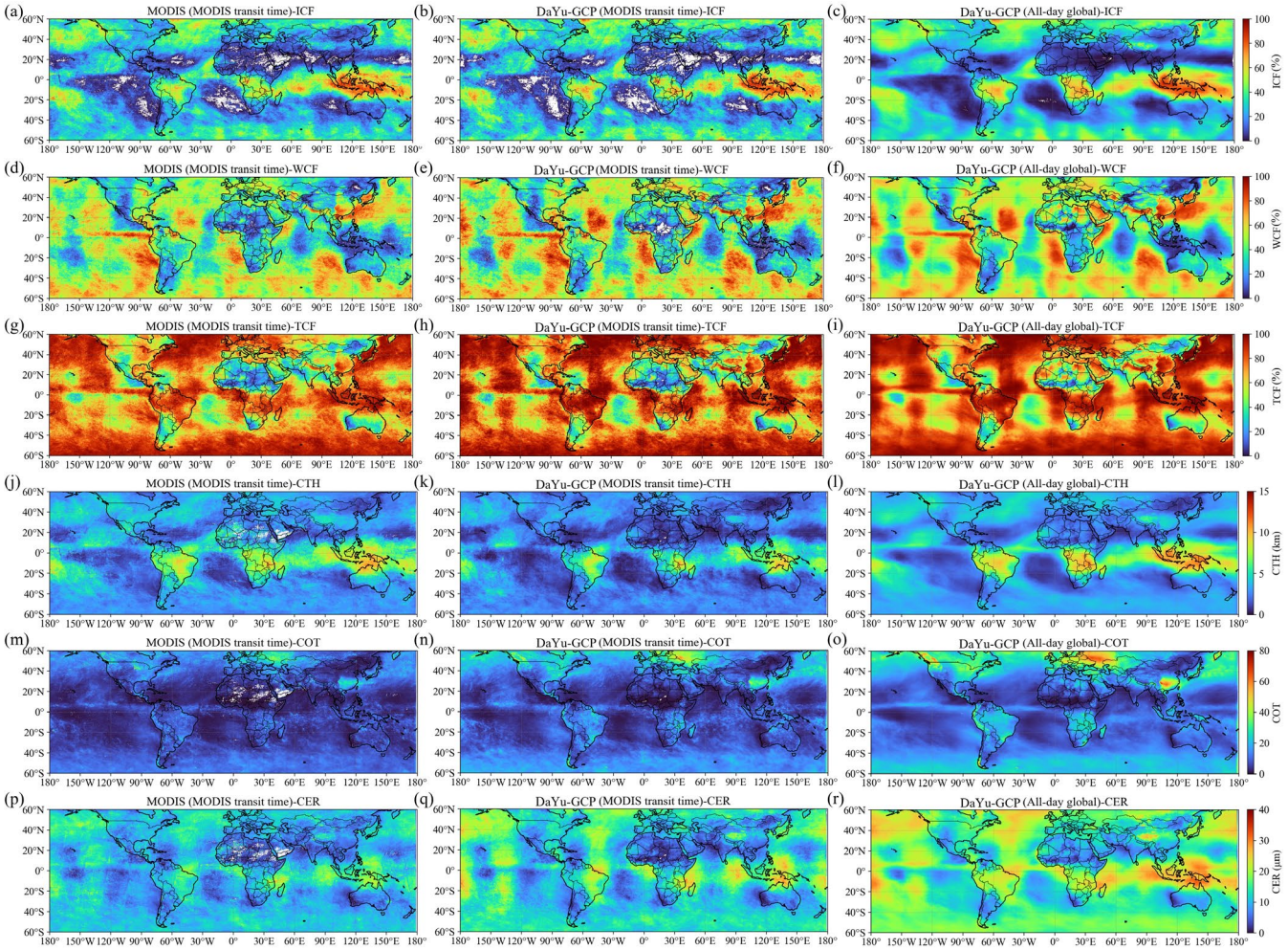

Figure S 1. The spatial distribution of global cloud physical products for the DJF season average from 2020 to 2022, respectively: ICF (a–c), WCF (d–f), TCF (g–i), CTH (j–l), COT (m–o), and CER (p–r). Vertically, these are the seasonal averages of the MODIS official cloud products with a 1.5 h transit time interval (a, d, g, j, m, p), the seasonal averages of DaYu-GCP at the same MODIS transit time and coverage location (b, e, h, k, n, q), and the seasonal averages of DaYu-GCP's all -day global products at all times (c, f, i, l, o, r).

Figure S2

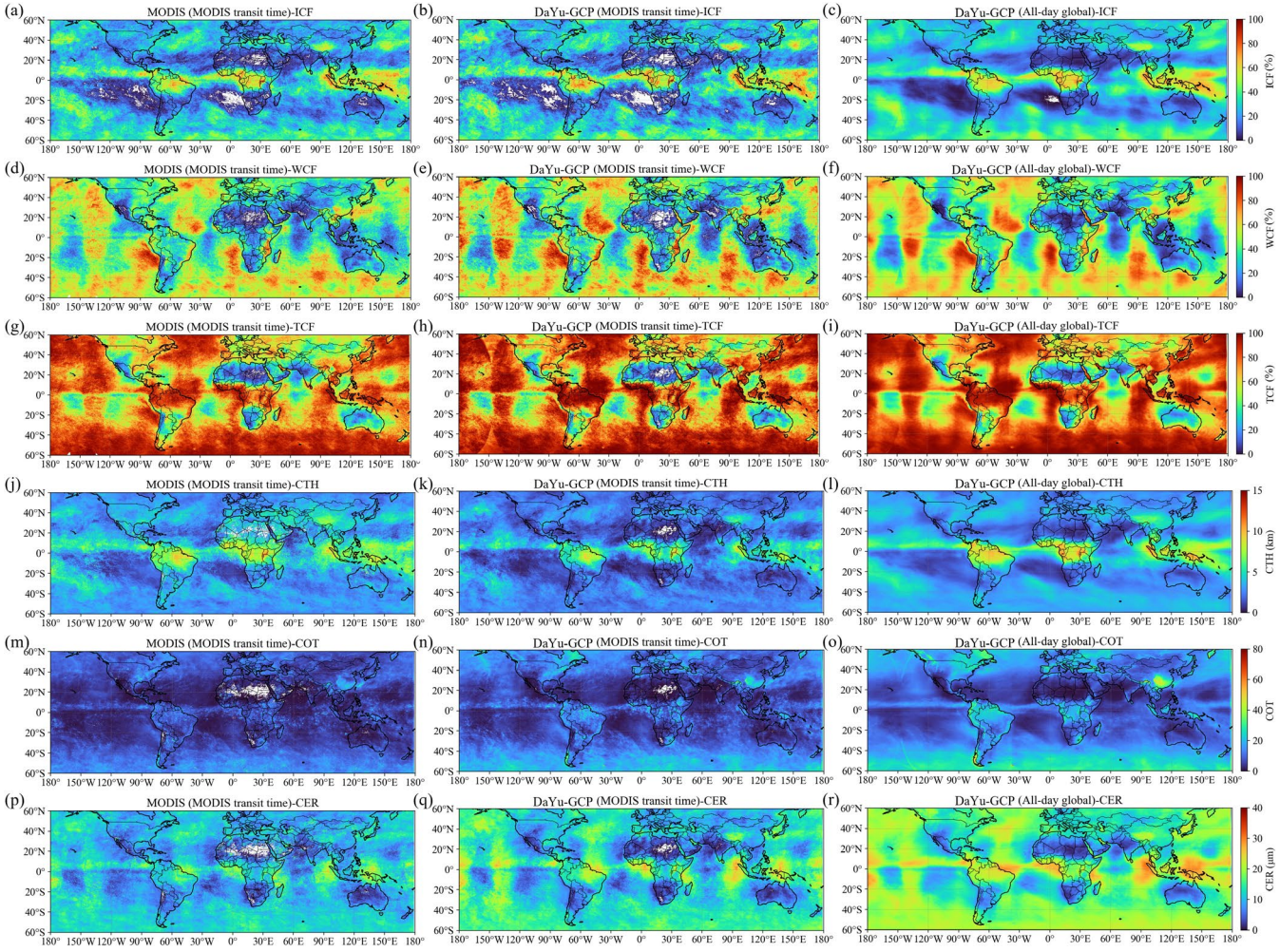

Figure S 2. The spatial distribution of global cloud physical products for the MAM season average from 2020 to 2022, respectively: ICF (a–c), WCF (d–f), TCF (g–i), CTH (j–l), COT (m–o), and CER (p–r). Vertically, these are the seasonal averages of the MODIS official cloud products with a 1.5 h transit time interval (a, d, g, j, m, p), the seasonal averages of DaYu-GCP at the same MODIS transit time and coverage location (b, e, h, k, n, q), and the seasonal averages of DaYu-GCP's all -day global products at all times (c, f, i, l, o, r).

Figure S3

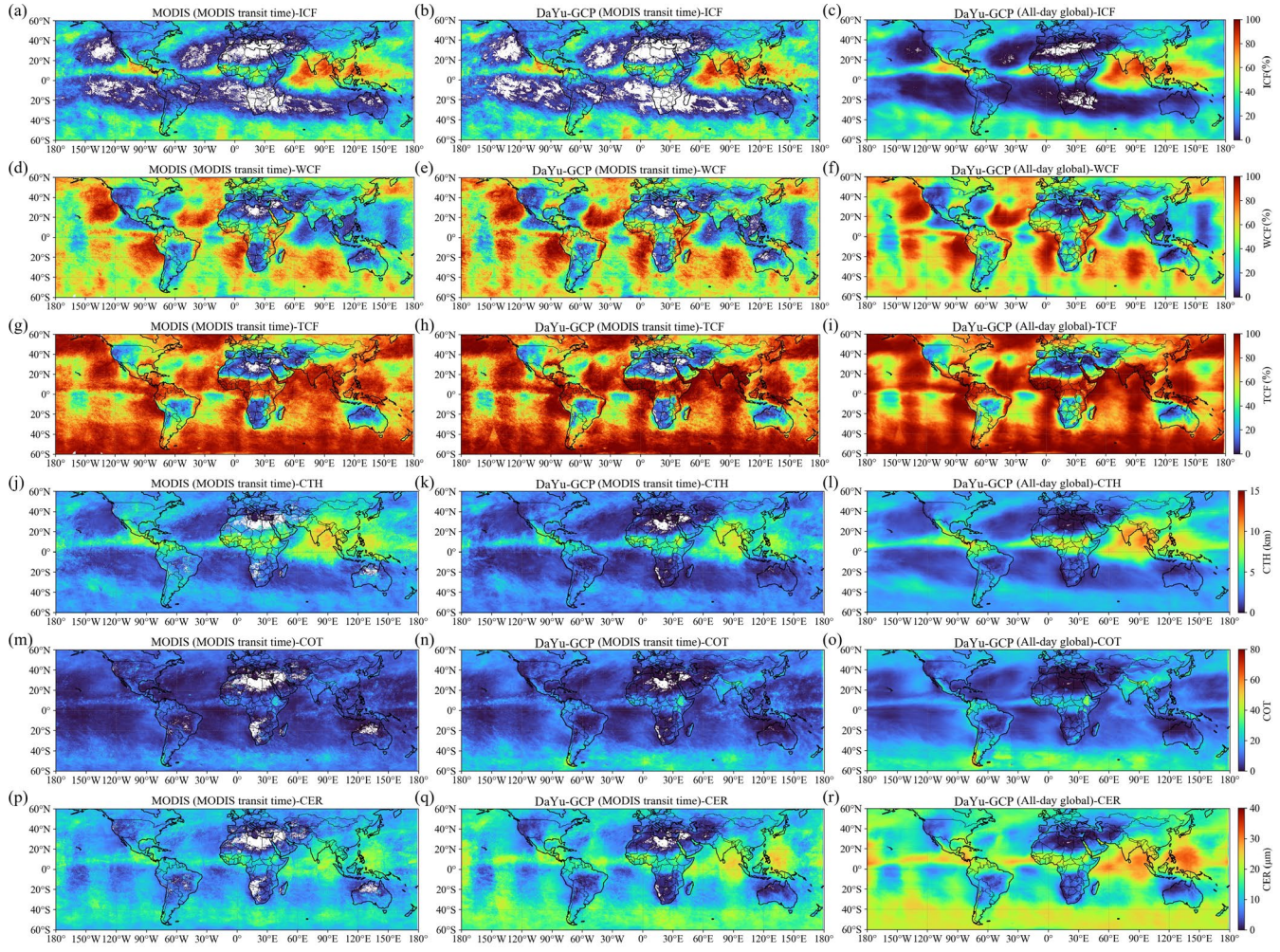

Figure S 3. The spatial distribution of global cloud physical products for the JJA season average from 2020 to 2022, respectively: ICF (a–c), WCF (d–f), TCF (g–i), CTH (j–l), COT (m–o), and CER (p–r). Vertically, these are the seasonal averages of the MODIS official cloud products with a 1.5 h transit time interval (a, d, g, j, m, p), the seasonal averages of DaYu-GCP at the same MODIS transit time and coverage location (b, e, h, k, n, q), and the seasonal averages of DaYu-GCP's all -day global products at all times (c, f, i, l, o, r).

Figure S4

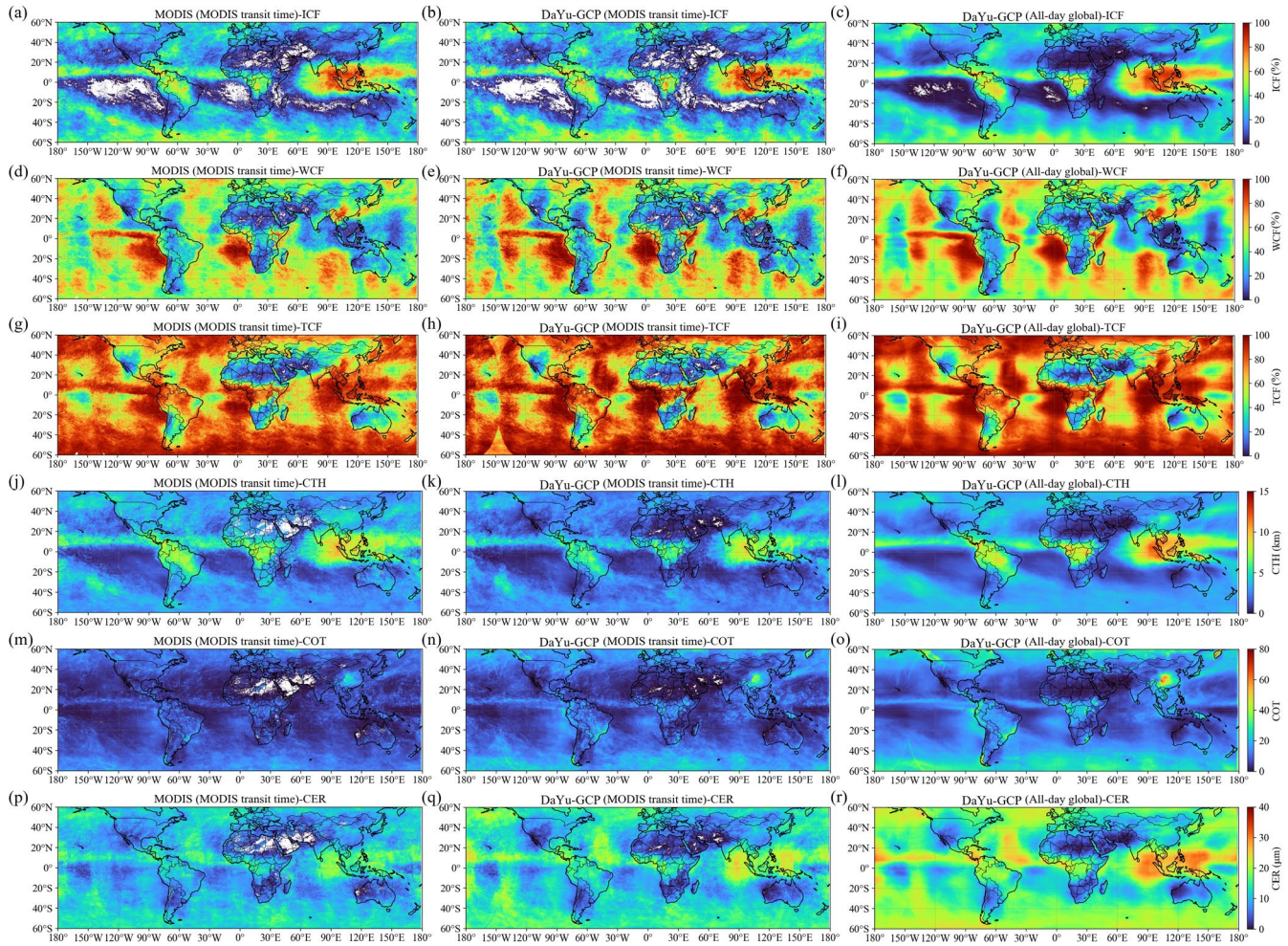

Figure S 4. The spatial distribution of global cloud physical products for the SON season average from 2020 to 2022, respectively: ICF (a–c), WCF (d–f), TCF (g–i), CTH (j–l), COT (m–o), and CER (p–r). Vertically, these are the seasonal averages of the MODIS official cloud products with a 1.5 h transit time interval (a, d, g, j, m, p), the seasonal averages of DaYu-GCP at the same MODIS transit time and coverage location (b, e, h, k, n, q), and the seasonal averages of DaYu-GCP's all -day global products at all times (c, f, i, l, o, r).